Journal of Sea Research 198 (2024) 102482

Contents lists available at ScienceDirect

Journal of Sea Research

journal homepage: www.elsevier.com/locate/seares

# GSDNet: A deep learning model for downscaling the significant wave height based on NAFNet

Xiaoyu Wu [a,b,c], Rui Zhao [a,b,c], Hongyi Chen [c], Zijia Wang [d], Chen Yu [c], Xingjie Jiang [b,e,f], Weiguo Liu [a], Zhenya Song [b,e,f,*]

[a] School of Software, Shandong University, Jinan 250101, China
[b] First Institute of Oceanography, and Key Laboratory of Marine Science and Numerical Modeling, Ministry of Natural Resources, Qingdao 266061, China
[c] Research Department, Computing Product Line, ICT Product & Solution, Huawei Technologies Co. Ltd., Hangzhou 310052, China
[d] College of Hydrology and Water Resources, Hohai University, Nanjing 210098, China
[e] Shandong Key Laboratory of Marine Science and Numerical Modeling, Qingdao 266061, China
[f] National Engineering Laboratory for Integrated Aero-Space-Ground-Ocean Big Data Application Technology, Xi'an 710072, China

ARTICLE INFO

*Keywords:*
Downscaling
Global location-specific transformation
Significant wave height
Deep learning
NAFNet

ABSTRACT

Finer resolution is one of the development trends in ocean surface waves simulation and forecasting. However, high-resolution numerical models for ocean surface waves have led to an enormous increase in computational complexity, posing a challenge with respect to balancing computational efficiency and timeliness. To meet the demand for refined ocean surface waves simulation/forecasting and to address the computational efficiency challenge of high-resolution ocean surface waves models, we propose a downscaling model called the Global location-Specific transformation Downscaling Network (GSDNet) based on the non-autoregressive fusion network (NAFNet). By incorporating global location-specific transformation and introducing a land–sea distribution indicator, GSDNet can quickly and accurately map low-resolution significant wave heights to high-resolution grids. The results show that, compared with traditional interpolation methods such as the bilinear, inverse distance weight interpolation (IDW), and bicubic methods, the GSDNet model can reduce the global mean absolute error (MAE) by >77%. Compared with those of FourCastNet (FCN), the Koopman neural operator (KNO), the original NAFNet, and residual networks in deep learning from empirical downscaling methods (DL4DS_ResNet), the MAE decreases by >21%. Furthermore, the GSDNet model outperforms the other downscaling methods at the coastal boundary and for identifying the maximum significant wave height. In this work, we provide an effective solution for balancing computational efficiency and timeliness, which is important for improving the accuracy and reliability of ocean surface waves simulation/forecasting.

## 1. Introduction

As an important physical phenomenon in the ocean, ocean surface waves (hereafter called wave) have a significant impact on various maritime activities, including ocean engineering, offshore oil extraction, fisheries, and maritime transportation. With the increase in maritime activities, the demand for accurate wave forecasting has been growing. Fine-scale wave forecasting can help reduce marine disasters, promote oceanographic research, and enhance marine forecasting services (Lavidas and Venugopal, 2018; Thomas and Dwarakish, 2015). The core tool for wave forecasting is numerical models. High-resolution wave numerical models, characterized by finer grids, can provide more detailed wave information and have become a major trend in wave modeling and forecasting. However, high-resolution wave models result in a significant increase in computational complexity (Qiao et al., 2016). In general, for each order-of-magnitude increase in the horizontal resolution, the computational workload increases by three orders of magnitude, posing challenges in terms of timeliness for weather forecasting and scientific research (Chawla et al., 2013). A balance between computational efficiency and timeliness has become a crucial and challenging issue in the pursuit of high-resolution modeling and forecasting.

* Corresponding author at: First Institute of Oceanography, and Key Laboratory of Marine Science and Numerical Modeling, Ministry of Natural Resources, Qingdao 266061, China.
*E-mail address:* songroy@fio.org.cn (Z. Song).

https://doi.org/10.1016/j.seares.2024.102482
Received 20 December 2023; Received in revised form 26 January 2024; Accepted 5 February 2024
Available online 6 February 2024

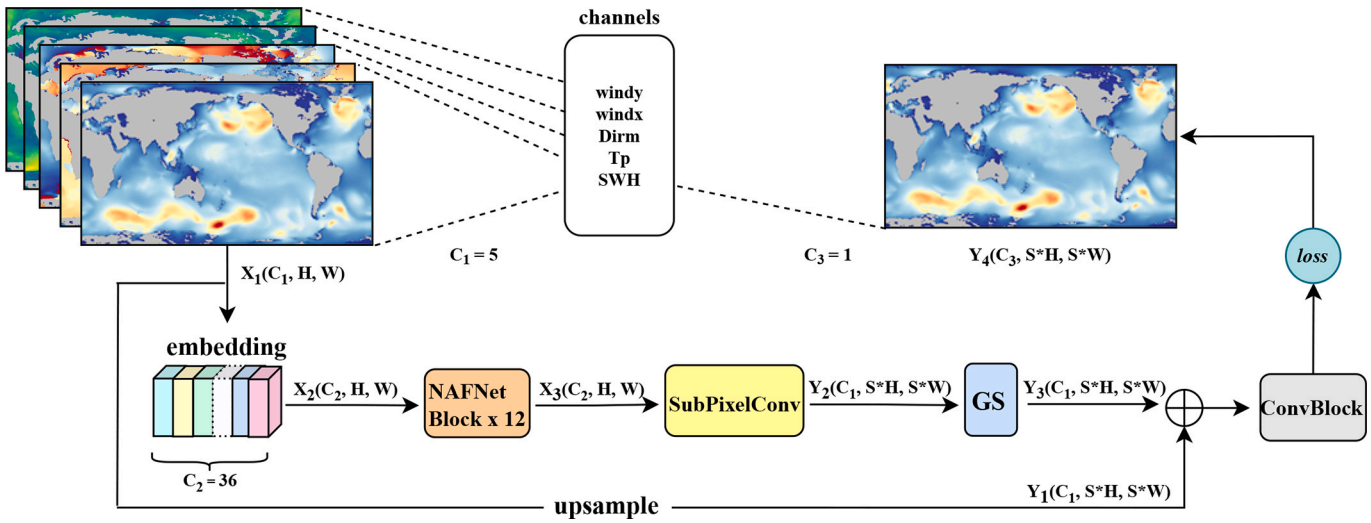


**Fig. 1.** The architecture of the Global location-Specific transformation Downscaling Network (GSDNet).

Downscaling is the process of transforming output information from large-scale, low-resolution models into small-scale, high-resolution information. Currently, there are two commonly used downscaling methods: dynamic downscaling and statistical downscaling (Jacobeit et al., 2014; Massaoudi et al., 2021). Dynamic downscaling involves the use of global or larger-scale low-resolution models to provide initial and boundary conditions for higher-resolution models in relatively smaller regions. By linking internal dynamics with other physical processes, dynamic downscaling can capture additional regional small-scale features while retaining the large-scale characteristics of global low-resolution models. Dynamic downscaling methods provide good physical meaning but require significant computational costs (Xu et al., 2019). Conversely, statistical downscaling relies on establishing statistical relationships between data elements at different resolutions based on historical data to derive high-resolution data. Common methods include interpolation methods (such as bilinear methods) and traditional statistical models (Hessami et al., 2008). However, traditional statistical downscaling methods do not accurately establish a mapping relationship between low-resolution observed data and high-resolution data, leading to poor accuracy and low reliability in simulation and forecasting (Massaoudi et al., 2021).

In recent years, with the development of deep learning, researchers have discovered that neural networks can be used to capture the nonlinear functional relationships between low-resolution and high-resolution data. Long short-term memory recurrent neural networks (RNN-LSTM) (Misra et al., 2018), convolutional neural networks (CNNs) (Pan et al., 2019), and other deep learning models have been applied for statistical downscaling (Baño-Medina et al., 2020) and have shown significant advantages over traditional statistical downscaling methods. In the field of deep learning, image superresolution (SR) is an important application for enhancing image and video resolutions (Wang et al., 2020) and further explores the mapping relationships between low-resolution and high-resolution data. The application of image SR in meteorology was first introduced by Vandal et al. (2017), who proposed a generalized deep-stacked SR convolutional network that significantly improved the downscaling ability compared with previous methods. The application of SR in the atmospheric sciences has been studied by Vandal et al. (2017), Leinonen et al. (2020), Kumar et al. (2021), Ooi and Ibrahim (2021). While these methods have shown promising results, they still have limitations, including poor spatial and temporal generalization and difficulties in capturing important features. Furthermore, research on downscaling significant wave heights is still in its early stages. Michel et al. (2022) used a CNN for the statistical downscaling of significant wave height predictions and observed better results than other statistical downscaling methods; however, their results still fall short of the performance of physical models. Adytia et al. (2022, 2023) proposed the use of LSTM and bidirectional LSTM to downscale significant wave heights in two marine regions near Indonesia; however, these methods did not perform well for enclosed regions. Currently, high-resolution global wave simulation and forecasting remain challenging.

To address the high-resolution modeling and forecasting of global significant wave heights, we propose a deep-learning downscaling model called the Global location-Specific transformation Downscaling Network (GSDNet) based on the non-autoregressive fusion network (NAFNet). This model incorporates a global location-specific transformation (GS), which enables accurate and high-performance mapping of low-resolution wave height data to a high-resolution grid. The proposed GSDNet model includes two main improvements.

1. The design of a global location-specific transformation allows the model to capture fine features in complex regions, thereby improving the downscaling ability at sea–land boundaries.
2. The accuracy of the overall model is further improved by introducing land (invalid points) and sea (valid points) distribution identifiers and eliminating all land points in the loss function.

The remainder of the paper is structured as follows. Section 2 introduces our data sources, methodology, and evaluation metrics, and in Section 3, we validate the effectiveness of the GSDNet model from multiple perspectives. In Section 4, we discuss the effect of network block hyperparameters on the accuracy and migration learning ability of the model to improve its generalizability and provide further suggestions and strategies to improve the accuracy and generalizability of the GSDNet model. Finally, in Section 5, we summarize our results and provide an outlook for future work.

## 2. Dataset and methods

### 2.1. Dataset

The experimental data in this work was obtained from the MASNUM-WAM model developed by the Key Laboratory of Marine Science and Numerical Modeling (MASNUM). MASNUM-WAM is a third-generation spectral wave model, which solves the energy spectrum balance equation in spherical coordinates and wavenumber space. And the ST6 source function package (Liu et al., 2017) is adopted to simulate the effects of wind input, white-capping dissipation, and swell dissipation on the evolution of waves (Jiang et al., 2023). It has been calibrated and

**Table 1**
Parameter settings for different deep learning downscaling methods.*

| | up_scale | embedding_size | num_blks | feature |
|---|---|---|---|---|
| FCN | 4 | 256 | 12 | 5 |
| KNO | 4 | 36 | 12 | 5 |
| DL4DS_ResNet | 4 | 64 | 8 | 5 |
| NAFNet | 4 | 36 | 12 | 5 |
| GSDNet | 4 | 36 | 12 | 5 |

* up_scale indicates the downscaling scale, embedding_size indicates the size of the initial embedding performed on the input data in the channel dimension (width of the neural network), num_blks indicates the number of blocks stacked in the neural network (one of the depth hyperparameters), and feature indicates the number of features in the input data.

adopted many times in wave simulations, and other scientific studies (Wang et al., 2016; Qiao et al., 2019; Bao et al., 2020; Song et al., 2020; Jiang et al., 2023). Therefore, validation of the MASNUM-WAM is not shown in this work.

In this work, model simulations were conducted at spatial resolutions of 1° × 1°, 1/2° × 1/2°, 1/4° × 1/4°, and 1/8° × 1/8° for the global wave field spanning 80° S–80° N and 0°–359° E in 2021. The spectral space is set to 24 directions in intervals of 15° with 35 wavenumbers equivalent to frequencies from 0.042 Hz to 1.073 Hz with a ratio of 1.1 at infinite depth. The wind-forcing data used in the simulations were obtained from the ECMWF-ERA5 reanalysis dataset with a temporal resolution of 1 h (Hersbach et al., 2020). For the downscaling model, we used five variables with 1 h temporal resolution derived from MASNUM outputs as the input, which are the significant wave height (SWH), peak wave period (Tp), mean wave direction (Dirm), zonal wind speed (windx), and meridional wind speed (windy). As a result, there are 8764 records for each variable from January 1 to December 31, 2021.

## 2.2. GSDNet model

### 2.2.1. Design principles and workflow

The GSDNet model is designed based on the NAFNet by incorporating a global location-specific transformation (GS) function (GS in Fig. 1), which considers the valid/invalid (sea/land) point distributions. The design of GS can capture fine features in margin regions to improve the downscaling ability at coastal boundaries and eliminate invalid (land) points in the loss function more easily.

A schematic of the structure of GSDNet is given in Fig. 1. Firstly, the input, low-resolution data $X_1(C_1, H, W)$, is upsampled (upsample in Fig. 1) by the superscaling ratio (S) to $Y_1(C_1, S*H, S*W)$. Here $C_1$ is the numbers of input channels, which is equal to 5 (SWH, Tp, Dirm, windx, windy). H and W are the numbers of grids in the latitudinal direction and longitude direction, respectively. Meanwhile, the input is embedded (embedding in Fig. 1) to $X_2(C_2, H, W)$, in which $C_2$ is the size of the initial embedding performed on the input data in the channel dimension (width of neutral network, embedding_size in Table 1) and set as 36 in this work. Secondly, following the NAFNet block for multiple feature extraction, $X_2(C_2, H, W)$ is mapped as $X_3(C_2, H, W)$. Thirdly, the sub-pixel convolution SubPixelConv is applied to the $X_3$ and then mapped output of the high-resolution data $Y_2(C_1, S*H, S*W)$. Fourthly, by using the global location-specific transformation (GS in Fig. 1), we can obtain $Y_3(C_1, S*H, S*W)$. Fifthly, sum the $Y_3$ and $Y_1$, and then feed into the output layer of the ConvBlock to obtain the final target high-resolution SWH $Y_4(C_3, S*H, S*W)$, in which $C_3$ is equal to 1 meaning we only select the first channel (SWH) data.

Here, the GSDNet model is further improved based on physical knowledge, i.e., by adding the ocean land identifier and using only the points of the ocean region (the dashed box in Fig. 2) in the calculation of the loss function. That is,

$$loss = \sum_{n=1}^{N} \left( I_{\{n\in\Xi\}} * \left( h_p(n) - h_m(n) \right) \right)^2, \quad (1)$$

where $h_p(n)$ and $h_m(n)$ denote the downscaling and true values of $n$ at the sample points, respectively; $N = N_{lon} \times N_{lat}$, where $N_{lon}$ and $N_{lat}$ are the numbers of meridional and latitudinal grids, respectively; and $I_{\{n\in\Xi\}}$ is the fitness function, i.e., $I_{\{n\in\Xi\}} = 1$ when sample point $n$ is a point in the ocean region; otherwise, $I_{\{n\notin\Xi\}} = 0$; and $\Xi$ denotes the set of sample points in all ocean regions.

### 2.2.2. Backbone selection

The upsampling method greatly impacts the accuracy of the super-scoring model; currently used upsampling methods consist of numerical upsampling and artificial intelligence (AI) upsampling. Numerical upsampling methods include bilinear interpolation, bicubic interpolation, and kriging interpolation. Although fast, numerical interpolation only involves simple operations based on low-resolution images to obtain high-resolution images, and these calculations can cause noise amplification and blurring of the results. The mainstream methods for AI upsampling are inverse convolution and subpixel convolution. Inverse convolution extends an image by inserting zeros and convolving them to obtain high-resolution images. Conversely, subpixel convolution directly expands the data in the channel dimension, and via periodic rearrangement, each pixel is decomposed into smaller pixels that are rearranged into high-resolution images according to certain rules (Shi et al., 2016). Overall, subpixel convolution is computationally small, fast, and effective and can avoid the blurring or checkerboard effects

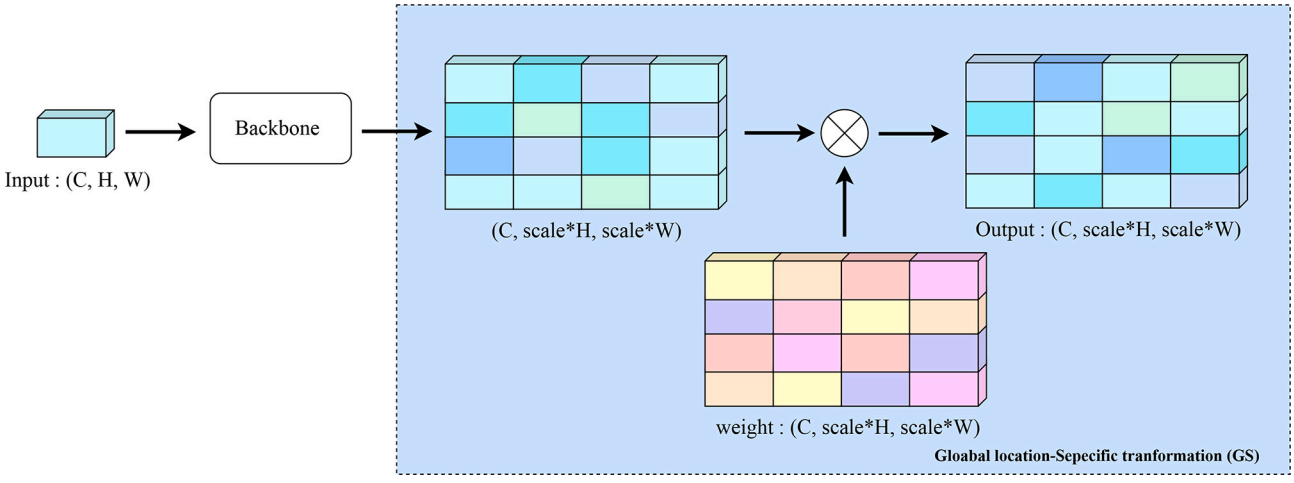


**Fig. 2.** Schematic of global location-specific transformation (GS), where C is the number of features in the data, H is the number of grids in the latitudinal direction, W is the number of grids in the longitudinal direction, and the scale is the superscaling ratio.

caused by numerical interpolation or inverse convolution. Accordingly, subpixel convolution was adopted in this study as the upsampling method for our downscaling model.

We also considered the location of the upsampling operation in the model. SR frameworks can be classified into four categories based on the location of upsampling in the model: preupsampling SR, postupsampling SR, stepwise upsampling SR, and iterative updownsampling SR. Considering the design complexity and training difficulty of stepwise upsampling and iterative upsampling, we chose a framework that combines the two methods of preupsampling and postupsampling.

Consequently, NAFNet was chosen as the baseline model; this model not only is powerful and concise for single-view feature extraction but can also fuse left- and right-view features via the cross-attention module (Chu et al., 2022). Its inputs are obtained by preupsampling and postupsampling the high-resolution data and the residuals of the high-resolution data, respectively, which reduces the spatiotemporal complexity and results in faster training and inference speeds (Wang et al., 2020). In this work, we selected the single-view feature extraction.

#### 2.2.3. Global location-specific transformation (GS)

Superscaling involves mapping low-resolution data to high-resolution data via neural networks, much like SR involves mapping low-resolution images to high-resolution images. However, the downscaling process involves not only fine-grained pixel filling of the image but also recalculation of the interactions between multiple elements (Li et al., 2023). The subpixel layer of the upsampling subpixel convolution approach proposed in the previous subsection has a larger receptive field, which provides more contextual information to help generate more realistic details. However, because the distribution of the receptive field is not uniform and the block regions actually share the same receptive field, this may lead to artifacts near the boundaries of different blocks, resulting in a limited ability to recover details. The image size can therefore be increased but not accurately enough to recover high-frequency details, especially for complex textures and sharp edges. In particular, in some of the topographically complex regions involved in the downscaling task, such as coastal boundaries and the Asia–Pacific intersection region, the computationally inclined smooth deep learning method has difficulty capturing complex geographic location features.

Accordingly, we propose a global location-specific transformation scheme that adds a locational transformation to each grid block based on its absolute location (Fig. 2). Mathematically, the entire feature map has a spatial resolution of $N_c \times N_{lon} \times N_{lat}$, where $N_c$, $N_{lon}$, and $N_{lat}$ denote the division of the data block along the feature axis and the longitude and latitude axes, respectively, into $N_c \times N_{lon} \times N_{lat}$ windows, each of which has a size of $1 \times 1 \times 1$. The global location-specific transformation matrix contains $N_c \times N_{lon} \times N_{lat}$ submatrices, each of which has one learnable parameter. By training the parameters of this global location-specific transformation matrix, different weights can be learned for different geographic locations. This approach enhances the ability of the downscaling method to identify features of complex terrains and can significantly improve the accuracy of the model. Moreover, the time complexity of this process is only $O(1)$, which means there is no additional time overhead.

### 2.3. Evaluation metrics

In this work, the data from the MASNUM-WAM simulation are treated as true values, and the model downscaling ability is evaluated using the mean absolute error (MAE), root mean square error (RMSE), and Pearson correlation coefficient (PCC), where the MAE and RMSE are used to assess the deviation of the downscaling values from the MASNUM data and the PCCs are used as measures of the correlation between the downscaling values and the MASNUM data. The above evaluation indicators are calculated as follows:

$$MAE = \frac{1}{i \cdot j}\sum_{i=1}^{I}\sum_{j=1}^{J}|h_p(i,j) - h_m(i,j)|, \tag{2}$$

$$RMSE = \sqrt{\frac{1}{i \cdot j}\sum_{i=1}^{I}\sum_{j=1}^{J}\left(h_p(i,j) - h_m(i,j)\right)^2}, \tag{3}$$

$$PCC = \frac{\sum_{i=1}^{I}\sum_{j=1}^{J}\left(h_p(i,j) - \overline{h_p(i,j)}\right)\left(h_m(i,j) - \overline{h_m(i,j)}\right)}{\sqrt{\sum_{i=1}^{I}\sum_{j=1}^{J}h_p\left((i,j) - \overline{h_p(i,j)}\right)^2\sum_{i=1}^{I}\sum_{j=1}^{J}\left(h_m(i,j) - \overline{h_m(i,j)}\right)^2}}, \tag{4}$$

where $i$ and $j$ denote the spatial grid point coordinates, $I$ denotes the total number of latitudinal grid points, $J$ denotes the total number of longitudinal grid points, $h_p(i,j)$ is the downscaling value of the model at point $(i,j)$, and $h_m(i,j)$ is the true value at point $(i,j)$. $\overline{h_p(i,j)}$ is the average of the model's downscaling values, and $\overline{h_m(i,j)}$ is the average of the true values.

This work also evaluated the downscaling ability of the model around the margin regions by coastal boundary error metrics. First, we define a coastal boundary point $(i,j)$, i.e., when $Hs(i,j) = 0$ and $Hs(i-1,j) + Hs(i+1,j) + Hs(i,j+1) + Hs(i,j-1) + Hs(i-1,j-1) + Hs(i-1,j+1) + Hs(i+1,j-1) + Hs(i+1,j+1) > 0$, we regard point $(i,j)$ as a shore boundary point. The error of the shoreline point $(i,j)$ is calculated as follows:

$$\mathrm{MAE(i,j)} = \mathrm{MAE}(\varphi) = \frac{1}{||\varphi||}\sum_{n\in\varphi}|h_p(n) - h_m(n)|, \tag{5}$$

where $\varphi = \{\{i-1,j\},\{i+1,j\},\{i,j+1\},\{i,j-1\},\{i-1,j-1\},\{i-1,j+1\},\{i+1,j-1\},\{i+1,j+1\}\}$ and $\|\varphi\|$ denote the number of elements in the set $\varphi$.

### 2.4. Experimental design

In addition to choosing NAFNet as a baseline model, traditional numerical interpolation methods such as inverse distance weight interpolation (IDW), bilinear interpolation (bilinear), and bicubic interpolation (bicubic) were also tested. The recently popular Koopman neural operator (KNO) model and FourCastNet (FCN) neural operator model were also served as comparison models in this work. In addition, we used residual networks (ResNets) constructed from deep learning from the empirical DownScaling (DL4DS) library (Gomez Gonzalez, 2023), which integrates cutting-edge downscaling algorithms, as a comparison model. ResNet adds a residual mechanism to traditional convolutional networks to alleviate the model degradation problem and is used in many supersegmentation models, including SRResNet, the deep recursive convolutional network for image superresolution (DRCN), and the multiscale residual network for image superresolution (MSRN) (Ledig et al., 2017; Kim et al., 2016; Li et al., 2018). For ease of illustration, we use the term DL4DS_ResNet to represent this model. The parameter settings for each depth model are given in Table 1.

As the characteristics of ocean surface waves may vary in different months, we divided the wave data for each month into training, validation, and testing sets in a ratio of 6:2:2 to ensure the reliability and generalization of the downscaling model. Therefore, the training, validation, and testing sets contain 5252, 1754, and 1754 records, respectively. Downscaling experiments with 1°-to-1/4° resolutions were then performed. Each downscaling method was built based on Python 3.8 and PyTorch 2.0, and 100 epochs were trained in a single A100 (traditional numerical interpolation models do not need to be trained).

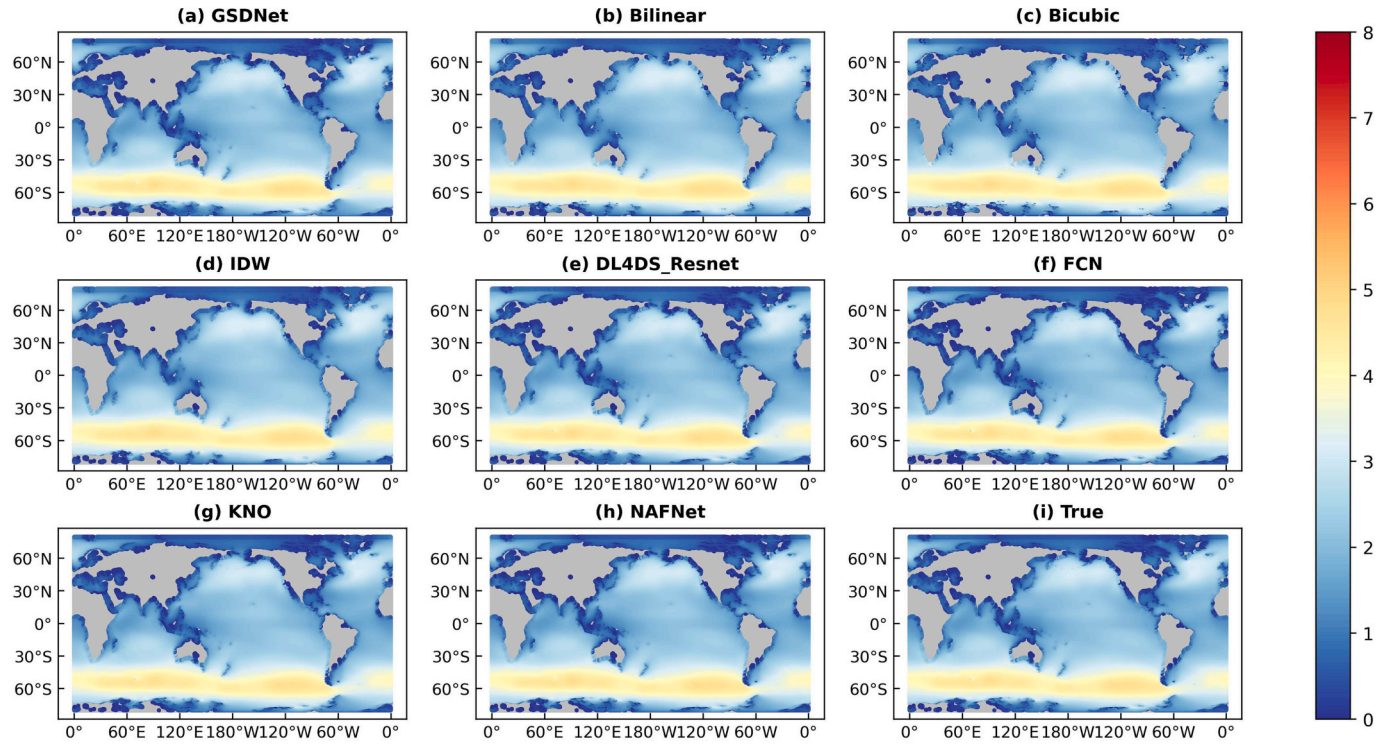


**Fig. 3.** Spatial distributions of (a)–(h) those generated by different downscaling methods, and (i) the true values (MASNUM wave model simulations) for the testing set.

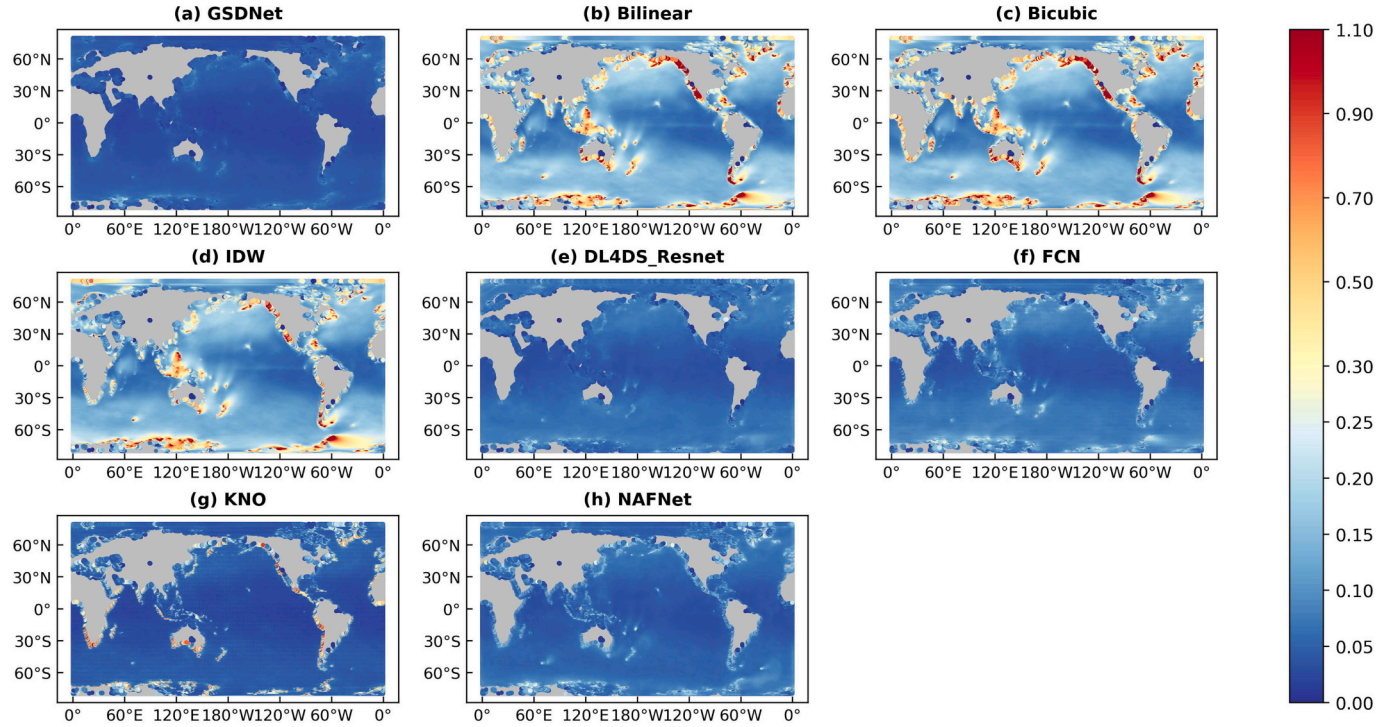


**Fig. 4.** Spatial distributions of the mean absolute error (MAE) of each downscaling method of the testing set. As seen from the colour bar on the right, blue indicates a smaller error, and red indicates a larger error. (For interpretation of the references to colour in this figure legend, the reader is referred to the web version of this article.)

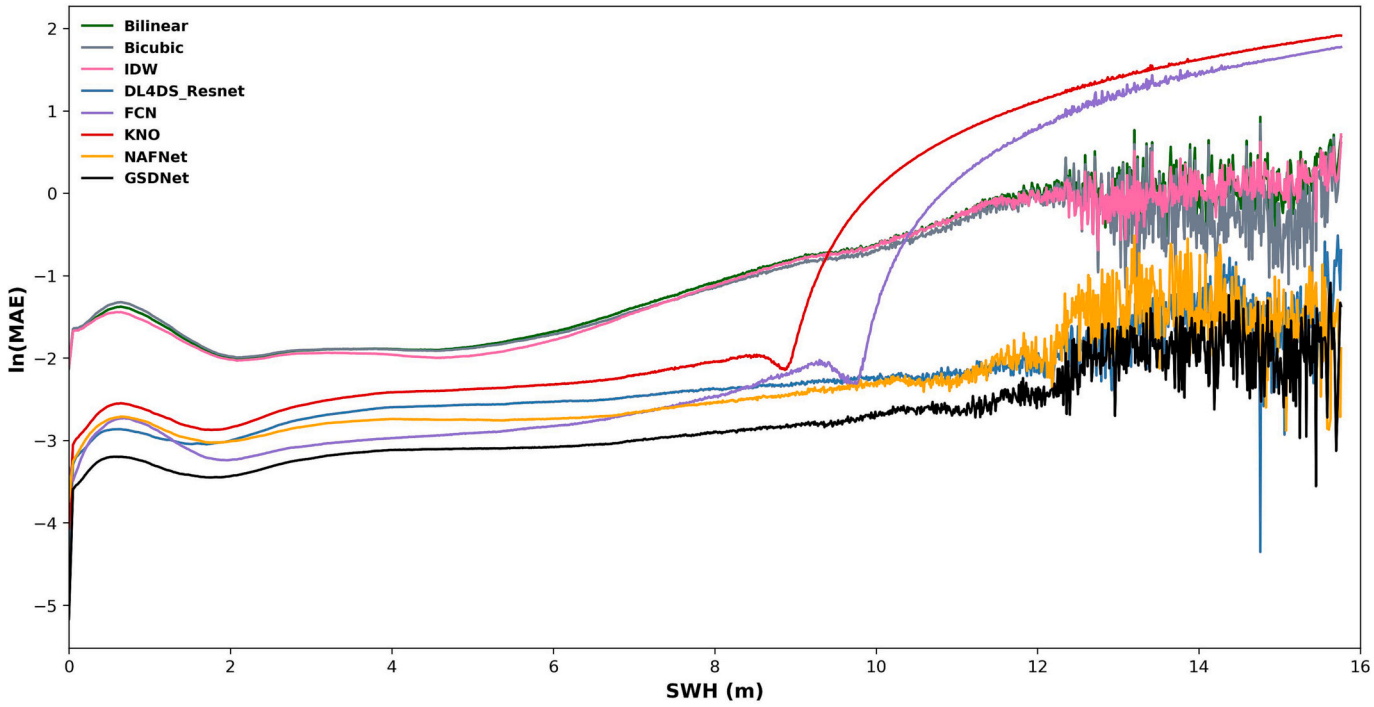


**Fig. 5.** Line plots of the downscaling ability of each downscaling method as a function of the significant wave height. The horizontal axis represents the true significant wave height, and the vertical axis represents the natural logarithm (ln) of the MAE between the model downscaling value and the true value. A larger value indicates a larger error. The black line indicates the GSDNet method.

## 3. Results

### 3.1. Evaluation of the global SWH downscaling ability

Fig. 3 shows the spatial distributions of the SWH mean of the true values (MASNUM-WAM model output with 1/4° resolution) of the entire testing set and the downscaling results obtained by each method. It seems that all downscaling methods can reproduce the major pattern of SWH distributions, such as larger SWH in the mid-high latitudes. However, from spatial distributions of the MAEs of each downscaling method (Fig. 4), it is clear that traditional numerical interpolation methods, such as bilinear (Fig. 4b), bicubic (Fig. 4c), and IDW (Fig. 4d) interpolations, generate results far from the true values because these interpolation methods use simple linear or quadratic polynomial interpolation, which cannot accurately map the complex nonlinear relationships between different resolutions. Compared with traditional numerical interpolation methods, the deep learning methods (Figs. 4a, and e-h) show a better downscaling ability, whose biases are closer to the true values. Moreover, the MAEs of GSDNet (Fig. 4a) are closer to 0 (dark blue) within the global ocean and are obviously better than those of the other models, suggesting that the GSDNet method is able to capture finer features.

To further explore the downscaling ability of GSDNet, the MAEs for each downscaling method as a function of SWH are shown in Fig. 5. The horizontal axis represents the true value of SWH, and the vertical axis represents the natural logarithm (ln) of the MAE between the downscaling value and the true value. Similarly to previous conclusions from the spatial distributions of the MAE, the traditional numerical interpolation methods show an obviously poor downscaling ability compared with deep learning methods. Among five deep learning methods, the downscaling errors of GSDNet (black line) are below 0.05 m (−3 in the vertical axis) and less than those of other downscaling methods (other colour lines) for the range of SWH from 0 m to 12 m. For the range of SWH from 12 m to 16 m, the GSDNet errors grow to 0.37 m (−1 in the vertical axis), but it still shows better downscaling ability than other methods, although GSDNet errors occur larger than those of NAFNet and DL4DS_ResNet at several points. It is interesting that the errors of neural operator models (FCN and KNO) increase rapidly earlier than other deep learning methods (DL4DS_Resnet, NAFNet, and GSDNet), which will be discussed in Section 3.3.

**Table 2**
Results of different downscaling methods on the evaluation indicators.

| Downscaling Method | MAE (Units: m) | RMSE (Units: m) | PCCs |
|---|---|---|---|
| Bilinear | 0.1640 | 0.2484 | 0.9820 |
| IDW | 0.1676 | 0.2541 | 0.9800 |
| Bicubic | 0.1668 | 0.2568 | 0.9808 |
| FCN | 0.0475 | 0.0862 | 0.9977 |
| KNO | 0.0711 | 0.1034 | 0.9966 |
| DL4DS_Resnet | 0.0582 | 0.0798 | 0.9979 |
| NAFNet | 0.0553 | 0.0783 | 0.9981 |
| GSDNet | **0.0372** | **0.0511** | **0.9991** |

The downscaling evaluation metrics also indicate that the GSDNet method has the lowest overall error and the highest correlation coefficient (Table 2). Decreases in the MAEs of 77.3%, 77.8%, and 77.7% and decreases in the RMSEs of 79.4%, 79.9%, and 80.1% are observed compared with those of the traditional bilinear, IDW, and bicubic interpolation methods, respectively. Compared with those of the FCN, KNO, and DL4DS_Resnet models, the GSDNet MAE decreases by 21.7%, 47.7%, and 36.1%, respectively, and the RMSE decreases by 40.1%, 50.6%, and 36.0%, respectively. Moreover, the 32.7% decrease in the MAE and 34.7% decrease in the RMSE compared with those of NAFNet indicate that GSDNet is able to capture more useful and detailed characteristics of SWH distributions by introducing global location-specific transformation. In general, GSDNet shows a better performance in the SWH downscaling compared to traditional interpolation methods and other deep learning methods.

### 3.2. Evaluation of the SWH downscaling ability in margin regions

A significant characteristic, as well as an advantage, of high-

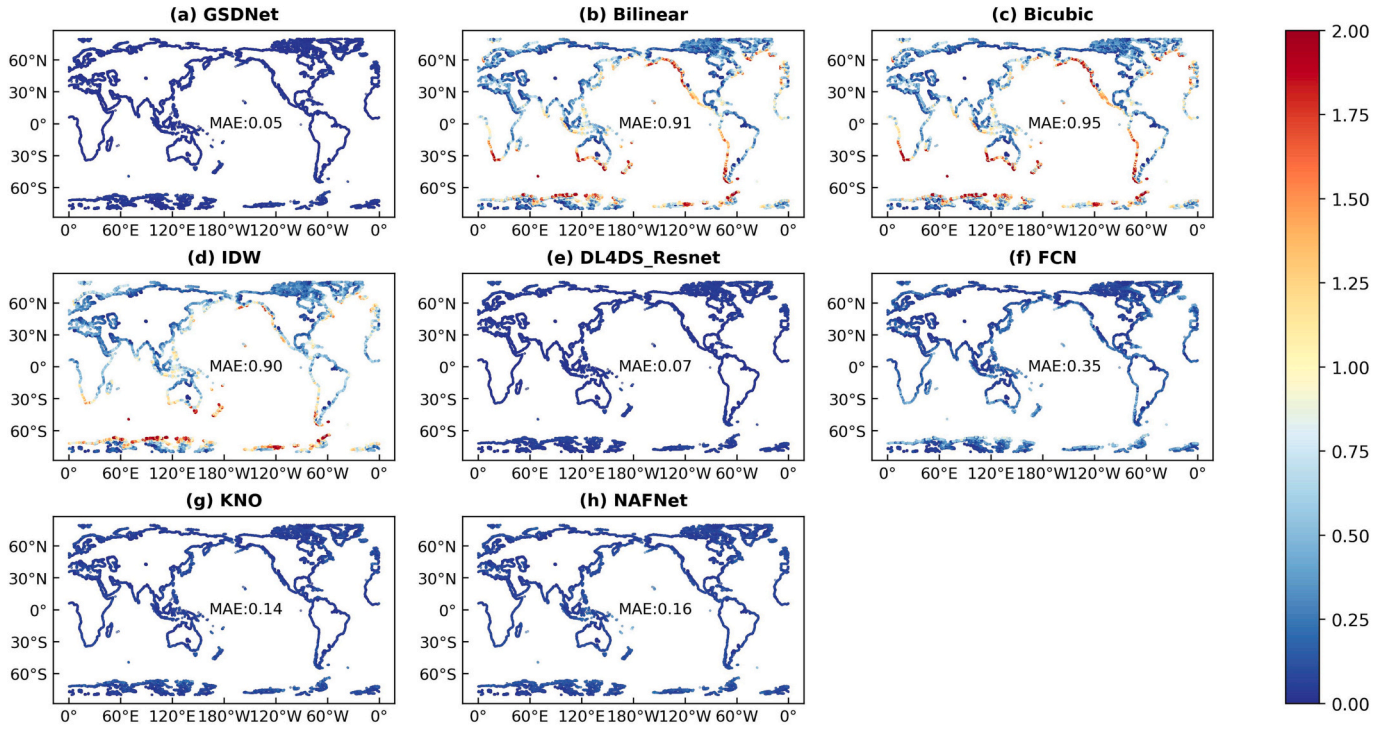


**Fig. 6.** Spatial distribution of the MAE for each downscaling method in the margin region across the testing set. Blue indicates smaller errors, and red indicates larger errors. (For interpretation of the references to colour in this figure legend, the reader is referred to the web version of this article.)

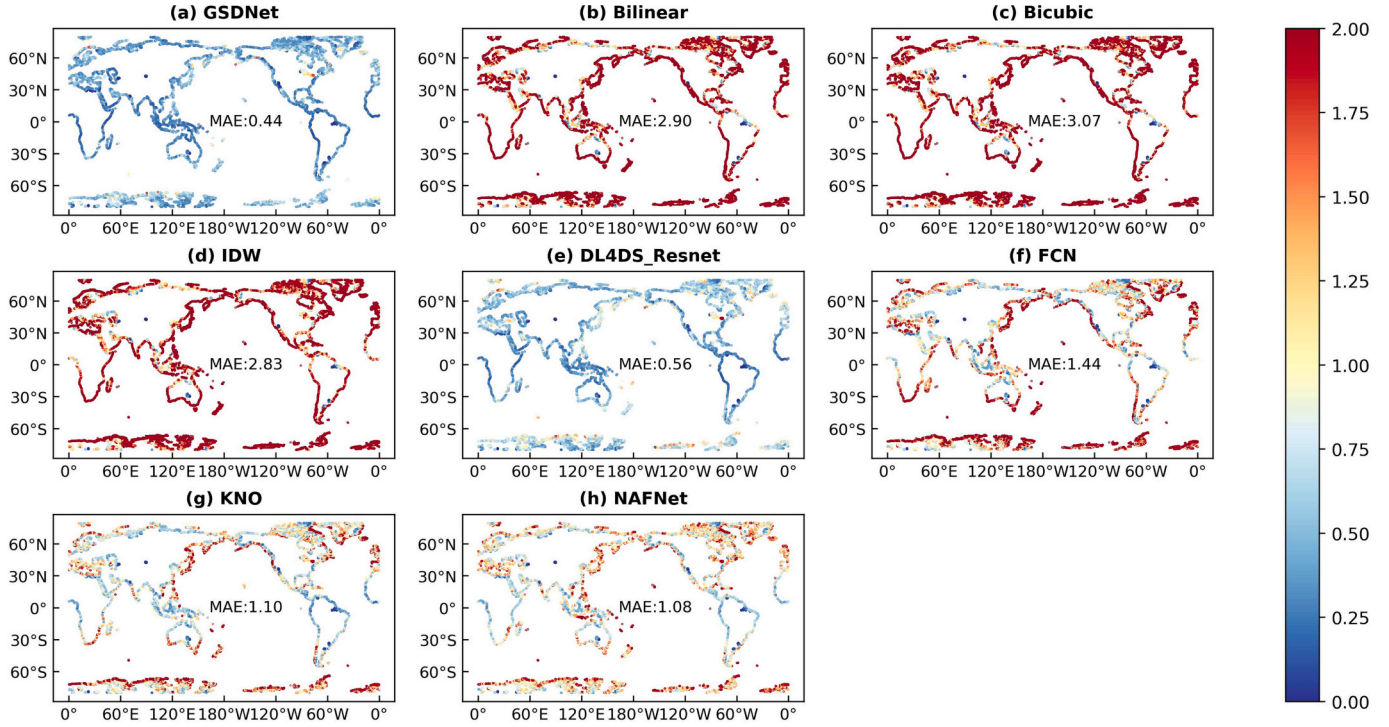


**Fig. 7.** Spatial distribution of the maximum absolute error values for each downscaling method for the margin region across the testing set. Blue indicates smaller errors, and red indicates larger errors. (For interpretation of the references to colour in this figure legend, the reader is referred to the web version of this article.)

resolution simulation/forecasting compared with low-resolution simulation/forecasting is the ability to provide a more detailed characterization of margin regions. Therefore, we conducted further analysis of the downscaling ability of different methods, specifically for margin regions. As shown in Fig. 6, the GSDNet (Fig. 6a) has the lowest error in the margin regions compared with the other downscaling methods. The MAEs of GSDNet are 94.5%, 94.7%, and 94.4% lower than those of the traditional bilinear (Fig. 6b), bicubic (Fig. 6c), and IDW (Fig. 6d) interpolation methods, respectively. The MAEs of GSDNet are 64.3%, 85.7%, and 28.6% lower than those of KNO (Fig. 6g), FCN (Fig. 6f), and DL4DS_ResNet (Fig. 6e), respectively, and 68.8% lower than those of NAFNet. To evaluate the performance and robustness of the models in

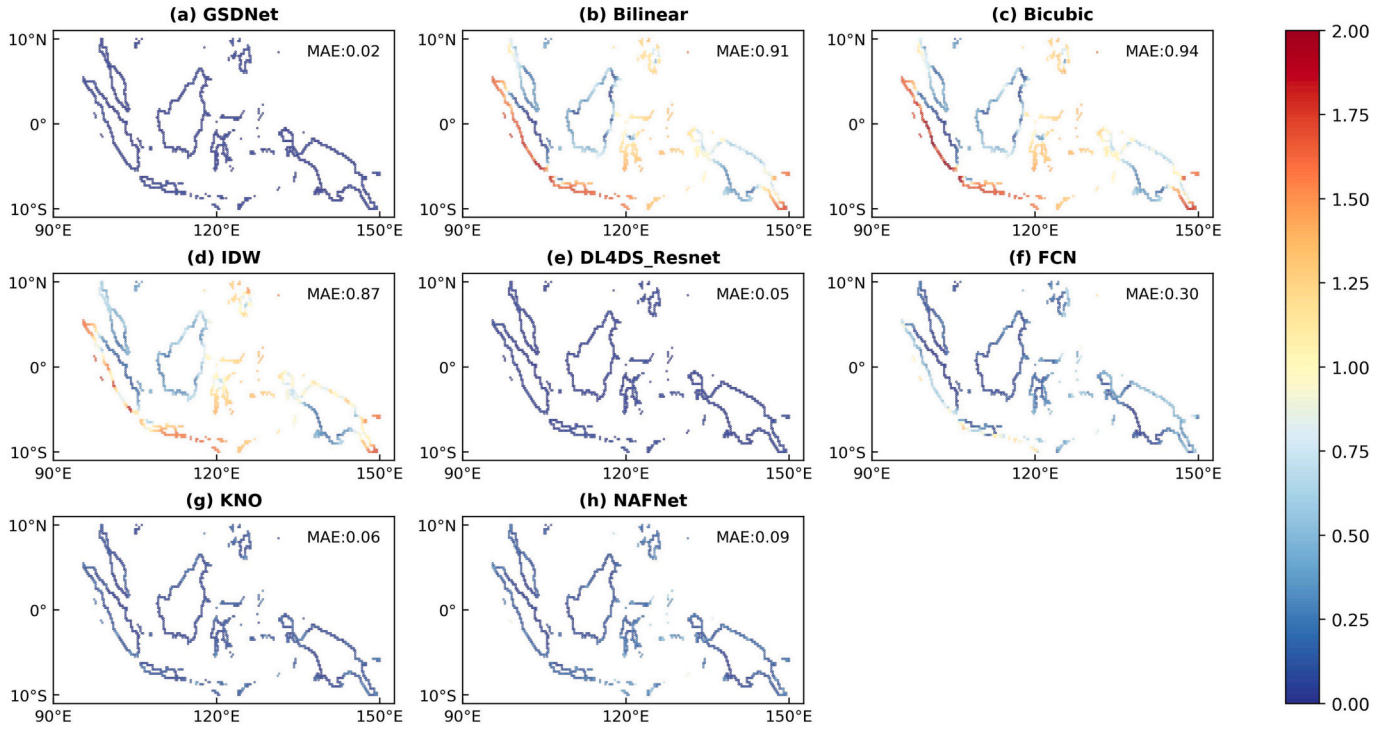


**Fig. 8.** Spatial distribution of MAEs for individual downscaling methods in the margin region at the Indo-Pacific convergence zone. Blue indicates smaller errors, and red indicates larger errors. (For interpretation of the references to colour in this figure legend, the reader is referred to the web version of this article.)

margin regions, we considered an extreme case and analyzed the maximum absolute error in the margin regions for the testing dataset (Fig. 7). The results show that the MAE of the maximum error in the margin regions for GSDNet (Fig. 7a) is only 0.44 m. In terms of the spatial distribution map colors and the MAE values, GSDNet clearly outperforms the other models, indicating a higher accuracy and reliability when downscaling the SWH in margin regions.

In particular, in the margin region of the Indo-Pacific convergence zone (Fig. 8), where the topography is very complex with many islands, the MAEs of the traditional numerical interpolation methods are all approximately 1 m, and those of the deep learning methods (except for the FCN), are all <0.1 m. However, the MAE of GSDNet is the smallest (0.02 m), which is lower than that of the other deep learning methods by >50%, demonstrating the effectiveness of the global location-specific transformation strategy proposed in this work.

The average and maximum errors for the margin regions and the average error for the coastal boundary in the Asia–Pacific convergence zone show that GSDNet could effectively capture the features of different regions to achieve the best results, followed by DL4DS_ResNet. Because of its weak feature recognition ability, while NAFNet can capture the general features of ocean regions, it has difficulty with margin regions with complex topography. The neural operator–based models FCN and KNO are better suited to the downscaling problem. However, the upsampling method using backconvolution generates ambiguous results because of zero filling, which is especially obvious in margin areas. The simple linear or quadratic polynomial interpolations used in traditional interpolation methods ignore complex topographic features and can not simulate the dynamics of the wave field.

### 3.3. Evaluation of the maximum-SWH downscaling ability

Accurate modeling and forecasting of the maximum SWH are critical for coastal safety, marine engineering and construction, and coastal protection. Accordingly, we identified the location of maximum value at each record in the testing set and analyzed the downscaling ability of each downscaling method at the location of maximum value to assess the ability of each downscaling method to simulate the maximum SWH. Fig. 9 shows a scatter plot of the downscaling results versus true values for each method at the location of the maximum value, and the linear relationship using the least squares method $y = kx + b$, where $x$ and $y$ are the downscaling results and true values, respectively. A value of $k$ closer to 1 corresponds to $b$ being closer to 0, indicating that the downscaling result of the method is closer to the true value. As shown in Fig. 9, traditional interpolation methods (Fig. 9b-d) use simple linear functions that cannot capture the nonlinear structure where the maxima are located. Thus, unsurprisingly, these methods perform poorly in terms of downscaling the maximum value. The neural operator models FCN (Fig. 9f) and KNO (Fig. 9g) have bottlenecks in terms of maximum value downscaling due to the inverse convolution operation, which may introduce pseudo-detail, handle edges and details inaccurately, and increase noise in the downscaling.

Interestingly, the downscaling maximum values of GSDNet (Fig. 9a), DL4DS_ResNet (Fig. 9e), and NAFNet (Fig. 9h) are basically the same. A possible reason is that all of them have adopted the residual mechanism in the model architecture, which can alleviate the vanishing gradient problem in the training process of the deep neural network through cross-layer connections and residual blocks. This architectural design helps to extract and represent the features related to the maxima in the input data, thus improving the downscaling of the maxima. We further compared the global spatial distributions of the maximum downscaling results of each method (Fig. 10) and found that GSDNet (Fig. 10a) had the smallest error in terms of the location of the maximum SWH in the margin regions, where its error was 34.2% lower than that of DL4DS_ResNet and 68.9% lower than that of NAFNet. In contrast, the traditional numerical interpolation methods had errors >3 m. The above analysis on the evaluation of maximum SWH shows that the GSDNet also has a good performance in extreme events downscaling.

## 4. Discussion

Next, we discuss the impact of the block size (one of the hyperparameters) on both the downscaling accuracy and speed. In addition,

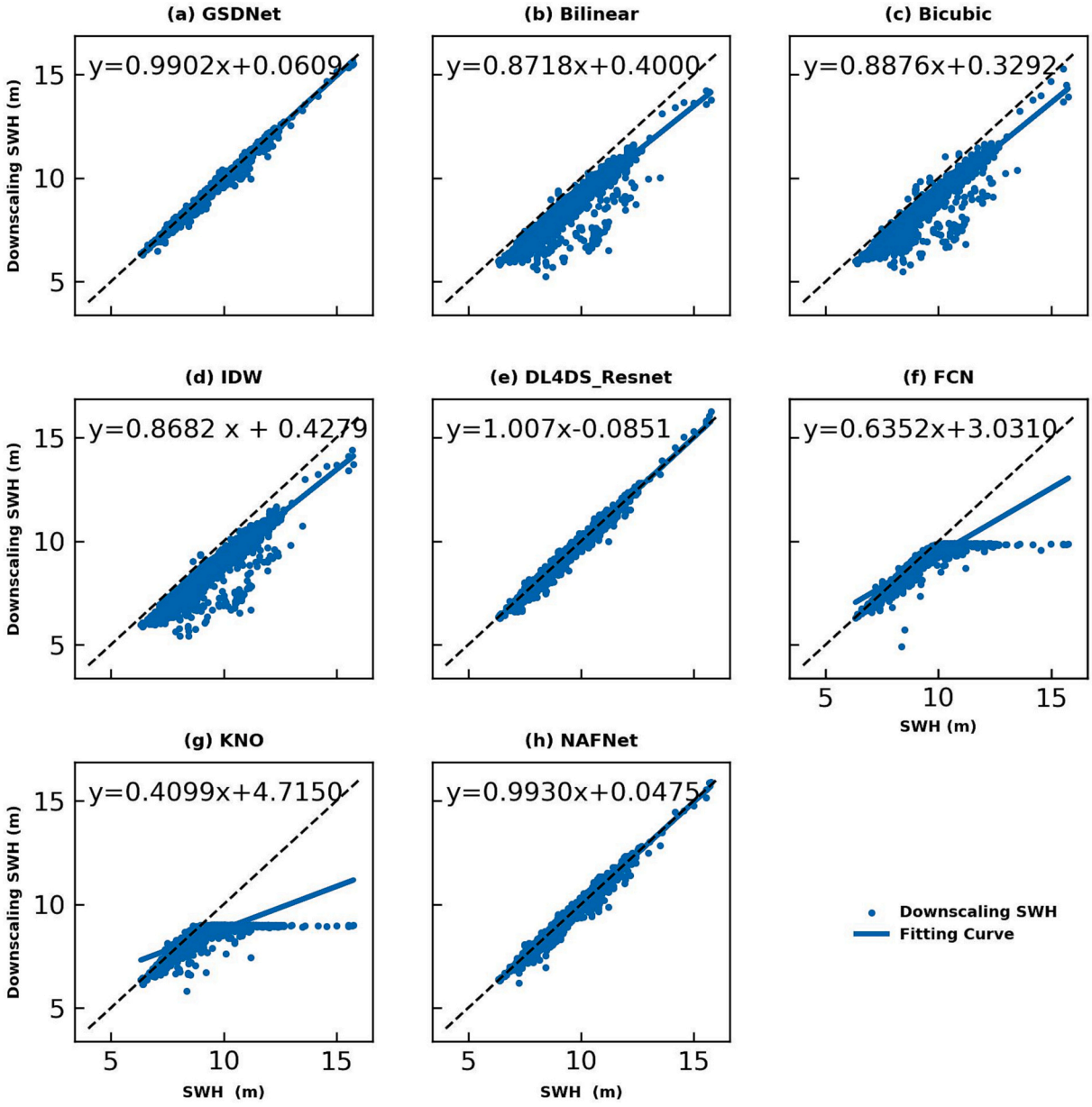


**Fig. 9.** Scatterplot of the downscaling results versus true values at the location of the maximum value in the testing set for each downscaling method. The horizontal axis represents the true value at the location of the maximum value, the vertical axis represents the downscaling value of the model at the location of the maximum value, and the dashed line in the middle represents the $y = x$ line, i.e., where the true value is equal to the downscaling value. The blue scatter indicates the relationship between the downscaling value and the true value of the downscaling method, and the blue straight line is the best-fit curve between the downscaling value and the true value. As the scatterplot and the fitted curve move closer to the dashed line, the downscaling value moves closer to the true value, and the downscaling improves. (For interpretation of the references to colour in this figure legend, the reader is referred to the web version of this article.)

we also examine the model's generalization ability at other resolutions.

### 4.1. Options to block size hyperparameter (num_blks)

The number of blocks stacked in the neural network (one of the depth hyperparameters) is one of the key hyperparameters, which may affect not only the downscaling accuracy but also the downscaling speed. How to balance the downscaling accuracy and speed is worth analyzing further. Therefore, we selected different values of the hyperparameter named num_blks of the GSDNet model (parameters in Table 1) ranging from 1 to 29 to find the relationships among the block size hyperparameter, downscaling accuracy, and downscaling speed (Fig. 11a). Here we use MAE to represent downscaling accuracy. The experiment results show that with increasing num_blks, the MAE (yellow line in Fig. 11a) gradually decreases while the downscaling time (blue line in Fig. 11b) gradually increases. Fitting the two curves using the least squares method (Fig. 11b), we find that the two fitted lines intersect when the num_blks is at 12.01. That is the reason that we set the num_blks as 12 in this work, which is the balance of downscaling accuracy and training speed. Certainly, without regard to the downscaling speed, the block size hyperparameter value (num_blks) can be further increased to improve the downscaling accuracy. Conversely, we can reduce the block size hyperparameter value to increase the downscaling speed.

### 4.2. Applicability of other resolutions

To analyze and evaluate the generalization ability of the GSDNet

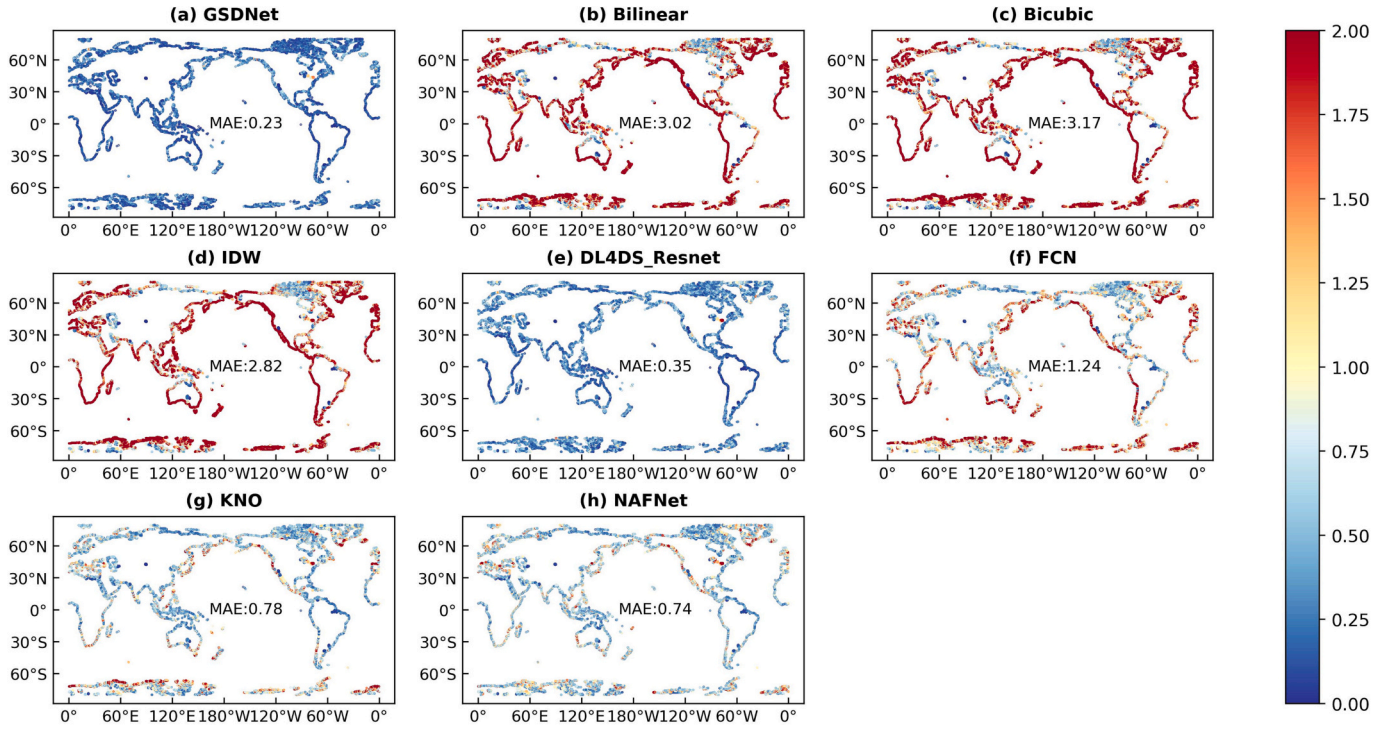


**Fig. 10.** Spatial distribution of the absolute errors in the downscaling of the maximum value in the margin regions for each downscaling method over the entire testing set. Blue indicates smaller errors, and red indicates larger errors. (For interpretation of the references to colour in this figure legend, the reader is referred to the web version of this article.)

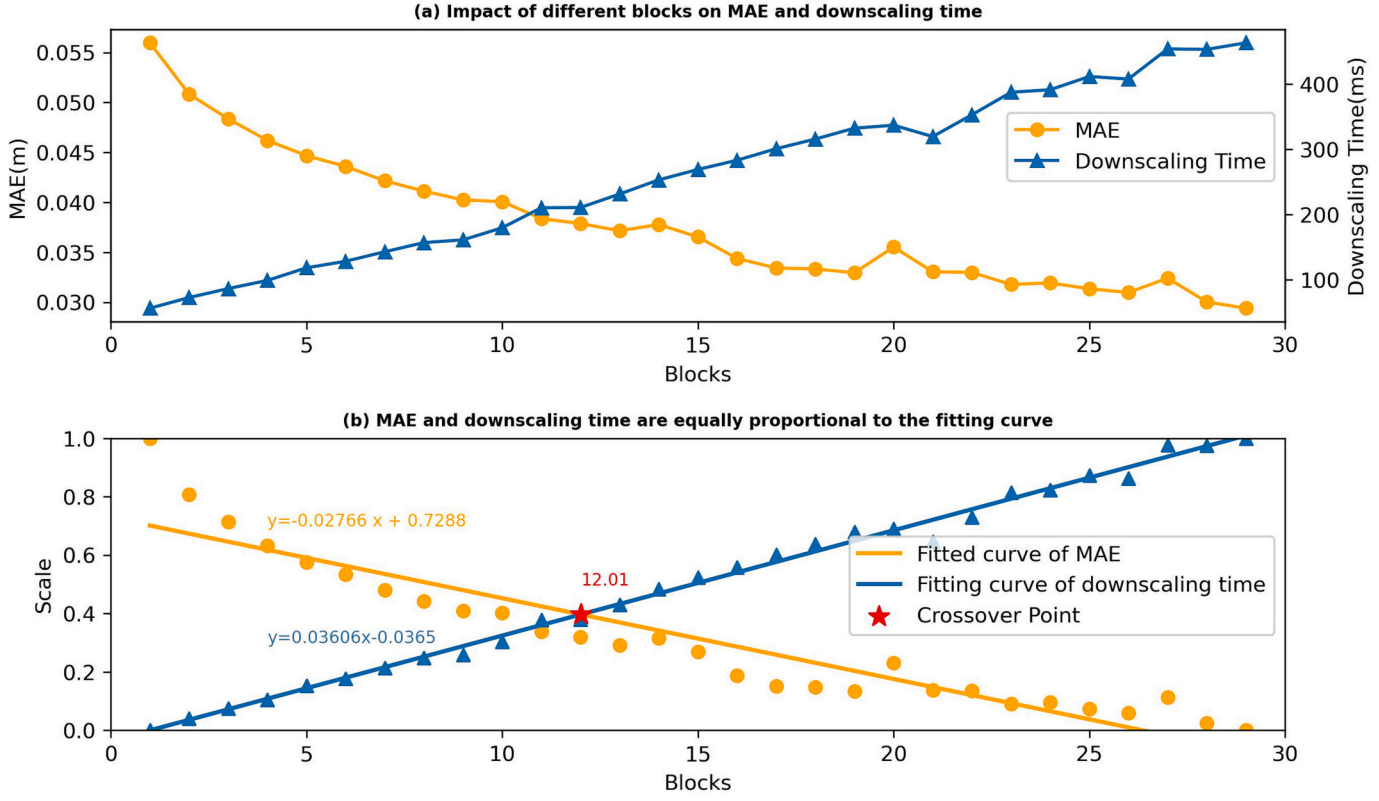


**Fig. 11.** Effect of the model block size hyperparameter on the model downscaling time and accuracy. (a) Double *y*-axis plot of the influence of the block size hyperparameter on the downscaling time and MAE, with the *x*-axis representing the number of stacked blocks of the neural network, the left *y*-axis representing the evaluation metric MAE, and the right *y*-axis representing the downscaling time. (b) Fitting curves of the downscaling time and MAE, mapping the double *y*-axis of Fig. (a) according to equal scales and then fitting the curve according to the least squares method. The red star represents the intersection point. (For interpretation of the references to colour in this figure legend, the reader is referred to the web version of this article.)

**Table 3**
Global location-Specific Transformation Downscaling Network (GSDNet) 1/2°-to-1/8° inference results with different fine-tuning settings.

| | MAE (Units: m) | RMSE (Units: m) | PCCs |
|---|---|---|---|
| GSDNet_NoneTrain | 0.2153 | 0.3037 | 0.9842 |
| GSDNet_Part | 0.0535 | 0.1167 | 0.9966 |
| GSDNet_Total | 0.0782 | 0.1370 | 0.9954 |

model deployed at other resolutions with the same downscaling ratio, we trained the model at 1°-to-1/4° resolutions and then applied for 1/2°-to-1/8° downscaling. To ensure an adequate amount of training and evaluation data, we selected 1400 records as the training set and 1000 records as the testing set. We carried out three sensitive experiments. The first experiment, named GSDNet_NoneTrain, used the GSDNet model trained at 1°-to-1/4° resolutions for the 1/2°-to-1/8° downscaling directly. The second experiment, named GSDNet_Total, used the GSDNet model trained at 1°-to-1/4° resolutions for downscaling after all model hyperparameters were fine-tuned on the 1/2°-to-1/8° training set. The third experiment, named GSDNet_Part, used the GSDNet model trained at 1°-to-1/4° resolutions for downscaling after the hyperparameters of the last two layers (GS and ConvBlock in Fig. 1) were fine-tuned on the 1/2°-to-1/8° training set.

As shown in Table 3, the GSDNet_NoneTrain experiment did not yield good results when directly inferring the 1/2°-to-1/8° resolution because the hyperparameters of the global-specific location transformation in the GSDNet model trained on the 1°-to-1/4° dataset are suitable only for the 1/4° grid and cannot be directly generalized to the 1/8° grid. Compared with GSDNet_NoneTrain experiment, both fine-tuning approaches effectively enabled GSDNet to generalize to the 1/8° grid. Moreover, both GSDNet_Total and GSDNet_Part converged within 10 epochs of training, significantly reducing the computational cost compared with training the downscaling model from scratch on a 1/2°-to-1/8° resolution. Fig. 12 shows the spatial distribution of the MAEs in the margin regions for the three experiments. Both GSDNet_Part (Fig. 12c) and GSDNet_Total (Fig. 12b) achieved good downscaling performance in the margin regions, while GSDNet_Part exhibited a particularly low MAE of only 0.09 m. It indicates GSDNet model captures the features of the SWH distributions between different resolutions.

It is interesting that GSDNet_Part performs better than GSDNet_Total. It may be due to the amount of the training data. We used 5252 records to train the GSDNet model downscaling from 1° to 1/4° resolutions. However, only a subset of data (1400 records in this work) was used to fine-tune the parameters because we want to deploy the trained model for other downscaling resolutions (1/2° to 1/8° in this work) at a low cost. Fewer trained data may lead to overfitting if we fine-tune all parameters of the model trained with more data. Certainly, if we used more data, such as 5252 records, the GSDNet_Total would perform better (not shown), but it would take longer training time and cost more training resources.

Note that there are various ways to perform fine-tuning and that we presented only two approaches here. We believe that with an appropriate fine-tuning strategy, even better results can be obtained.

## 5. Conclusions

In this work, we proposed a downscaling model, GSDNet, which can map low-resolution global significant wave heights to high-resolution significant wave heights with high accuracy and performance. The 1°-to-1/4° experiments show that the fine features in complex regions can be well captured by including the global location-specific transformation strategy, and the downscaling ability of GSDNet is better than that of traditional interpolation methods and other deep learning methods.

Compared with the Bilinear, IDW, and bicubic numerical interpolation methods, the MAEs of SWH are reduced by >77%. Compared with the FCN, KNO, NAFNet, and DL4DS_Resnet deep learning methods, the MAEs of SWH decreased by >21%, and their RMSEs decreased by >34.0%. The MAEs over the margin regions for the GSDNet model are >94% lower than those of the bilinear, IDW, and bicubic methods and >28% lower than those of the KNO, FCN, NAFNet, and DL4DS_Resnet methods. Moreover, GSDNet achieved better results in downscaling the maximum SWH, and the biases in the margin regions were reduced by >34% compared with that of the other methods. And, in the coastal boundary of the Indo-Pacific convergence zone, which features complex topography, the GSDNet reduced the MAEs by >97% compared with traditional numerical interpolation methods and by >60% compared with the FCN, KNO, NAFNet, and DL4DS_Resnet deep learning methods.

The experiments of generalization ability, in which GSDNet model was trained at 1°-to-1/4° resolutions and then applied for 1/2°-to-1/8° downscaling, show the GSDNet model captures the features of the SWH distributions between different resolutions and lies an extensive application perspective for SWH downscaling using low computational cost fine-tuning strategy (i.e., freezing the underlying weights and retaining only specific layers for training for several epochs).

This work is a good attempt at SWH downscaling, and GSDNet showed the potential application in wave downscaling. However, there are still several issues that need further study. Firstly, the data used in this work is only from a single year (2021), so the generalization performance needs to be evaluated further. Secondly, the hyperparameters, both the width and depth of the neural network, play important roles in model results. We only discussed the effects of num_blks (one of the depth hyperparameters) on downscaling results. The width (embedding_size) and the joint effects need to be analyzed further. Thirdly, additional wave parameters, such as wave period and wave direction, are also important for ocean science research and engineering. We will develop a joint downscaling model for wave parameters based on GSDNet by increasing the number of output channels, and try to apply it to other fields, e.g., ocean temperature downscaling. Fourthly, the GSDNet model remains a supervised deep learning model. In fact, as obtaining high-resolution data is still a challenge, we should pay more attention to unsupervised deep learning models for downscaling in the

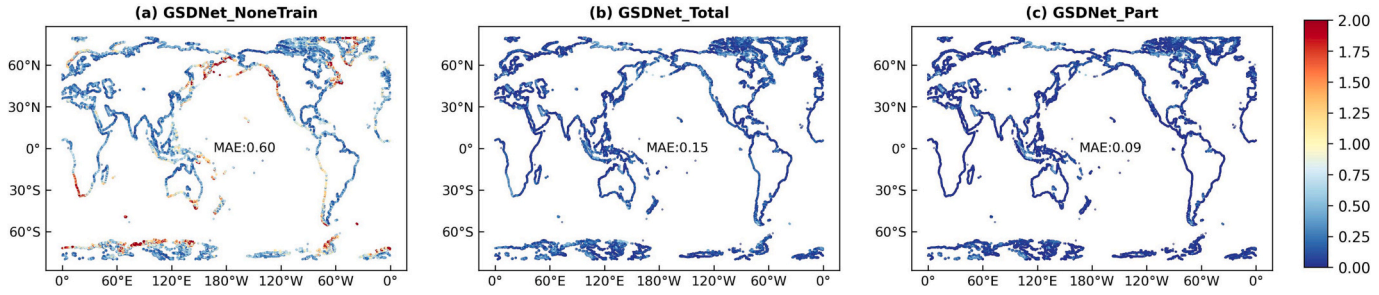


**Fig. 12.** Spatial distribution of the global shoreline downscaled MAEs for GSDNet under different fine-tuning settings: (a) GSDNet_NoneTrain, (b) GSDNet_Total, and (c) GSDNet_Part.

future.

## CRediT authorship contribution statement

**Xiaoyu Wu:** Writing – original draft, Visualization, Software, Methodology, Formal analysis. **Rui Zhao:** Writing – review & editing, Validation, Software. **Hongyi Chen:** Writing – review & editing, Validation, Methodology. **Zijia Wang:** Writing – review & editing, Investigation, Data curation. **Chen Yu:** Writing – review & editing, Resources, Project administration, Conceptualization. **Xingjie Jiang:** Writing – review & editing, Data curation. **Weiguo Liu:** Writing – review & editing, Project administration. **Zhenya Song:** Writing – review & editing, Supervision, Resources, Funding acquisition, Formal analysis, Conceptualization.

## Declaration of competing interest

The authors declare that they have no known competing financial interests or personal relationships that could have appeared to influence the work reported in this paper.

## Data availability

Data will be made available on request.

## Acknowledgments

We wish to thank the editor and two anonymous reviewers for their valuable suggestions and comments. This work was supported by Laoshan Laboratory (LSKJ202202100), Basic Scientific Fund for National Public Research Institute of China (Shu-Xingbei Young Talent Program 2023S01), the National Natural Science Foundation of China (42022042 and 41821004), and the China–Korea Cooperation Project on Northwest Pacific Marine Ecosystem Simulation under Climate Change.

## References

Adytia, D., Saepudin, D., Pudjaprasetya, S.R., Husrin, S., Sopaheluwakan, A., 2022. A deep learning approach for wave forecasting based on a spatially correlated wind feature, with a case study in the Java Sea, Indonesia. Fluids 7 (1), 39. https://doi.org/10.3390/fluids7010039.

Adytia, D., Saepudin, D., Tarwidi, D., Pudjaprasetya, S.R., Husrin, S., Sopaheluwakan, A., Prasetya, G., 2023. Modelling of deep learning-based downscaling for wave forecasting in coastal area. Water 15 (1), 204. https://doi.org/10.3390/w15010204.

Baño-Medina, J., Manzanas, R., Gutiérrez, J.M., 2020. Configuration and intercomparison of deep learning neural models for statistical downscaling. Geosci. Model Dev. 13 (4), 2109–2124. https://doi.org/10.5194/gmd-13-2109-2020.

Bao, Y., Song, Z., Qiao, F., 2020. FIO-ESM version 2.0: model description and evaluation. J. Geophys. Res. Oceans 125. https://doi.org/10.1029/2019JC016036 e2019JC016036.

Chawla, A., Tolman, H.L., Gerald, V., Spindler, D., Spindler, T., Alves, J.G.M., Cao, D., Hanson, J.L., Devaliere, E., 2013. A multigrid wave forecasting model: a new paradigm in operational wave forecasting. Weather Forecast. 28 (4), 1057–1078. https://doi.org/10.1175/WAF-D-12-00007.1.

Chu, X., Chen, L., Yu, W., 2022. NAFSSR: stereo image super-resolution using NAFNet. In: Proceedings of the IEEE Conference on Computer Vision and Pattern Recognition (CVPR), 1239-1248. https://doi.org/10.48550/arXiv.2204.0871.

Gomez Gonzalez, C.A., 2023. DL4DS—deep learning for empirical downscaling. Environ. Data Sci. 2, E3. https://doi.org/10.1017/eds.2022.26.

Hersbach, H., Bell, B., Berrisford, P., Hirahara, S., Horányi, A., Muñoz-Sabater, J., Nicolas, J., Peubey, C., Radu, R., Schepers, D., Simmons, A., Soci, C., Abdalla, S., Abellan, X., Balsamo, G., Bechtold, P., Biavati, G., Bidlot, J., Bonavita, M., De Chiara, G., Dahlgren, P., Dee, D., Diamantakis, M., Dragani, R., Flemming, J., Forbes, R., Fuentes, M., Geer, A., Haimberger, L., Healy, S., Hogan, R.J., Hólm, E., Janisková, M., Keeley, S., Laloyaux, P., Lopez, P., Lupu, C., Radnoti, G., de Rosnay, P., Rozum, I., Vamborg, F., Villaume, S., Thépaut, J.N., 2020. The ERA5 global reanalysis. Q. J. R. Meteorol. Soc. 146, 1999–2049. https://doi.org/10.1002/qj.3803.

Hessami, M., Gachon, P., Ouarda, T.B.M.J., St-Hilaire, A., 2008. Automated regression-based statistical downscaling tool. Environ. Model Softw. 23 (6), 813–834. https://doi.org/10.1016/j.envsoft.2007.10.004.

Jacobeit, J., Hertig, E., Seubert, S., Lutz, K., 2014. Statistical downscaling for climate change projections in the Mediterranean region: methods and results. Reg. Environ. Chang. 14 (6), 1891–1906. https://doi.org/10.1007/s10113-014-0605-0.

Jiang, X., Xie, B., Bao, Y., Song, Z., 2023. Global 3-hourly wind-wave and swell data for wave climate and wave energy resource research from 1950 to 2100. Scientific Data 10, 225. https://doi.org/10.1038/s41597-023-02151-w.

Kim, J., Lee, J.K., Lee, K.M., 2016. Deeply-recursive convolutional network for image super-resolution. In: Proceedings of the IEEE Conference on Computer Vision and Pattern Recognition (CVPR), 1637-1645. https://doi.org/10.48550/arXiv.1511.04491.

Kumar, B., Chattopadhyay, R., Singh, M., Chaudhari, N., Kodari, K., Barve, A., 2021. Deep learning–based downscaling of summer monsoon rainfall data over Indian region. Theor. Appl. Climatol. 143, 1145–1156. https://doi.org/10.1007/s00704-020-03489-6.

Lavidas, G., Venugopal, V., 2018. Application of numerical wave models at European coastlines: a review. Renew. Sust. Energ. Rev. 92, 489–500. https://doi.org/10.1016/j.rser.2018.04.112.

Ledig, C., Theis, L., Huszar, F., Caballero, J., Cunningham, A., Acosta, A., Aitken, A., Tejani, A., Totz, J., Wang, Z., Shi, W., 2017. Photo-realistic single image super-resolution using a generative adversarial network. In: Proceedings of the IEEE Conference on Computer Vision and Pattern Recognition (CVPR), 4681-4690. https://doi.org/10.48550/arXiv.1609.04802.

Leinonen, J., Nerini, D., Berne, A., 2020. Stochastic super-resolution for downscaling time-evolving atmospheric fields with a generative adversarial network. IEEE Trans. Geosci. Remote Sens. 59 (9), 7211–7223. https://doi.org/10.1109/TGRS.2020.3032790.

Li, J., Fang, F., Mei, K., Zhang, G., 2018. Multi-scale residual network for image super-resolution. In: Proceedings of the European Conference on Computer Vision (ECCV), 517-532. https://doi.org/10.1007/978-3-030-01237-3_32.

Li, T., Chang, H., Mishra, S., Zhang, H., Katabi, D., Krishnan, D., 2023. Mage: masked generative encoder to unify representation learning and image synthesis. In: Proceedings of the IEEE Conference on Computer Vision and Pattern Recognition (CVPR), 2142-2152. https://doi.org/10.48550/arXiv.2211.09117.

Liu, Q., Babanin, A., Fan, Y., Zieger, S., Guan, C., Moon, I.J., 2017. Numerical simulations of ocean surface waves under hurricane conditions: assessment of existing model performance. Ocean Model 118, 73–93. https://doi.org/10.1016/j.ocemod.2017.08.005.

Massaoudi, M., Abu-Rub, H., Refaat, S.S., Chihi, I., Oueslati, F.S., 2021. Deep learning in smart grid technology: a review of recent advancements and future prospects. IEEE Access 9, 54558–54578. https://doi.org/10.1109/ACCESS.2021.3071269.

Michel, M., Obakrim, S., Raillard, N., Ailliot, P., Monbet, V., 2022. Deep learning for statistical downscaling of sea states. Adv. Stat. Climatol. Meteorol. Oceanogr. 8, 83–95. https://doi.org/10.5194/ascmo-8-83-2022.

Misra, S., Sarkar, S., Mitra, P., 2018. Statistical downscaling of precipitation using long short-term memory recurrent neural networks. Theor. Appl. Climatol. 134 (3–4), 1179–1196. https://doi.org/10.1007/s00704-017-2307-2.

Ooi, Y.K., Ibrahim, H., 2021. Deep learning algorithms for single image super-resolution: a systematic review. Electronics 10 (7), 867. https://doi.org/10.3390/electronics10070867.

Pan, B., Hsu, K., AghaKouchak, A., Sorooshian, S., 2019. Improving precipitation estimation using convolutional neural network. Water Resour. Res. 55 (3), 2301–2321. https://doi.org/10.1029/2018WR024090.

Qiao, F., Zhao, W., Yin, X., Huang, X., Liu, X., Shu, Q., Wang, G., Song, Z., Li, X., Liu, H., Yang, G., Yuan, Y., 2016. A highly effective global surface wave numerical simulation with ultra-high resolution. In: Proceedings of the International Conference for High Performance Computing, Networking, Storage and Analysis (SC '16), pp. 46–56. https://doi.org/10.1109/SC.2016.4.

Qiao, F., Wang, G., Khokiattiwong, S., Akhir, M., Zhu, W., Xiao, B., 2019. China published ocean forecasting system for the 21st-Century Maritime Silk Road on December 10, 2018. Acta Oceanol. Sin. 38, 1–3. https://doi.org/10.1007/s13131-019-1365-y.

Shi, W., Caballero, J., Huszar, F., Totz, J., Aitken, A.P., Bishop, R., Rueckert, D., Wang, Z., 2016. Real-time single image and video super-resolution using an efficient sub-pixel convolutional neural network. In: Proceedings of the IEEE Conference on Computer Vision and Pattern Recognition (CVPR), 1874-1883. https://doi.org/10.48550/arXiv.1609.05158.

Song, Z., Bao, Y., Zhang, D., Shu, Q., Song, Y., Qiao, F., 2020. Centuries of monthly and 3-hourly global ocean wave data for past, present, and future climate research. Scientific Data 7, 226. https://doi.org/10.1038/s41597-020-0566-8.

Thomas, T.J., Dwarakish, G.S., 2015. Numerical wave modelling–a review. Aquatic Procedia 4, 443–448. https://doi.org/10.1016/j.aqpro.2015.02.059.

Vandal, T., Kodra, E., Ganguly, S., Michaelis, A., Nemani, R., Ganguly, A.R., 2017. DeepSD: Generating high resolution climate change projections through single image super-resolution. In: Proceedings of the 23rd ACM SIGKDD International Conference on Knowledge Discovery and Data Mining, pp. 1663–1672. https://doi.org/10.1145/3097983.3098004.

Wang, G., Zhao, C., Xu, J., Qiao, F., Xia, C., 2016. Verification of an operational ocean circulation-surface wave coupled forecasting system for the China's sea. Acta Oceanol. Sin. 35, 19–28. https://doi.org/10.1007/s13131-016-0810-4.

Wang, Z., Chen, J., Hoi, S.C., 2020. Deep learning for image super-resolution: a survey. IEEE Trans. Pattern Anal. Mach. Intell. 43 (10), 3365–3387. https://doi.org/10.1109/TPAMI.2020.2982166.

Xu, Z., Han, Y., Yang, Z., 2019. Dynamical downscaling of regional climate: a review of methods and limitations. Sci. China Earth Sci. 62, 365–375. https://doi.org/10.1007/s11430-018-9261-5.